# Supporting Information

Verho et al. 10.1073/pnas.1204328109

## SI Text

**Energetics of the Micro-Cassie to Nano-Cassie Transition.** Calculating the free energy difference of the micro-Cassie and nano-Cassie states is no different from calculating the Cassie-Wenzel transition energy for a single level topography, except that the equilibrium (Cassie-Baxter) contact angle of the nanofilaments has to be taken as the Young's contact angle of the microposts. The free energy change during the transition is

$$\Delta G = (\gamma_{sl} - \gamma_s)\Delta A_{sl} + \gamma \Delta A_l, \qquad [S1]$$

where $\Delta A_{sl}$ is the increase of solid-liquid contact area and $\Delta A_l$ is the change of liquid-air interfacial area. $\gamma$, $\gamma_s$ and $\gamma_{sl}$ are the liquid-air, solid-air and liquid-solid interfacial tensions, respectively. Using $A_b$ as the area of the bottom in a unit cell and $2\pi r_p h$ as the area of the post sidewalls, we arrive at, using the Young's equation $\cos\theta_Y = (\gamma_s - \gamma_{sl})/\gamma$,

$$\Delta G = \gamma(-\cos\theta_Y(A_b + 2\pi r_p h) - A_b). \qquad [S2]$$

The micro-Cassie state is energetically favorable if $\Delta G > 0$. This is the case if

$$\cos\theta_Y < -\frac{A_b}{A_b + 2\pi r_p h}. \qquad [S3]$$

For the micropattern discussed in this study, with a post height of 5 μm, the inequality is satisfied with $\theta_Y$ larger than 132°. The equilibrium contact angle of the nanofilament coating is clearly larger than this, which implies that the micro-Cassie is the lower energy state.

**Micro-Cassie to Nano-Cassie Transition.** By a force balance consideration, we can calculate the critical Laplace pressure $\Delta p_c$ for the micro-Cassie to nano-Cassie transition. The transition occurs when the meniscus depins from the edges of the posts and moves toward the bottom (see Fig. S1*A*). We proceed under the assumption that the shape of the meniscus around each post is approximately identical across the area under the water jet, which is reasonable because the diameter of the water jet is much larger than the size scale of the micropattern. The downward force per unit cell exerted on the meniscus by the Laplace pressure is

$$F_{lp} = A_b \Delta p, \qquad [S4]$$

where $\Delta p$ is the Laplace pressure. The balancing upward force caused by surface tension at the edges of the posts has the value

$$F_\gamma = -2\pi r_p \gamma \cos\theta, \qquad [S5]$$

where $\theta$ is the contact angle that the meniscus makes with the sidewall of the post. In equilibrium $F_\gamma = F_{lp}$. The forces are largest when $\theta$ equals the advancing contact angle of the sidewalls $\theta_A$ (the advancing contact angle of the nanofilament coating). The Laplace pressure is then

$$\Delta p_c = -\frac{2\pi r_p}{A_b}\gamma\cos\theta_A. \qquad [S6]$$

The advancing contact angle of the nanofilament coating is roughly 170°, which gives $\Delta p_c = 6.9$ kPa. For comparison, for single level topography with a fluorinated coating with an advancing angle of 120° one gets $\Delta p_c = 3.5$ kPa.

**Axisymmetric Meniscus Shape.** Consider the microscopic meniscus on the sidewall of a micropost shown in Fig. S1*B*. Assuming cylindrical symmetry, we write the vertical force balance for the part of the meniscus indicated in the figure. The surface tension on the contact line acts to pull the meniscus upwards, while the Laplace pressure $\Delta p$ and the surface tension at $r$ tend to push the meniscus toward the bottom. The force balance reads

$$\pi(r^2 - r_p^2)\Delta p + 2\pi r_p \gamma\cos\theta + 2\pi r\gamma\sin\alpha = 0, \qquad [S7]$$

where $r_p$ is the post radius and $\gamma$ is the surface tension. The sine of $\alpha$ can be expressed in terms of the derivative $\mathrm{d}z/\mathrm{d}r$ as

$$\sin\alpha = \left(1 + \frac{1}{(\mathrm{d}z/\mathrm{d}r)^2}\right)^{-\frac{1}{2}}. \qquad [S8]$$

Inserting [**S8**] into [**S7**] yields

$$\frac{\mathrm{d}z}{\mathrm{d}r} = -\left[\left(\frac{r}{r_p\cos\theta + \frac{\Delta p}{2\gamma}(r^2 - r_p^2)}\right)^2 - 1\right]^{-1}. \qquad [S9]$$

This result will be used below. In addition, we remark that this equation can also be used to calculate approximate shapes of the meniscus close to the micro-Cassie to nano-Cassie transition, although in reality the shape will not be perfectly axisymmetric.

**Air Pockets at the Bases of the Posts.** During a Cassie-Wenzel transition, the water immediately wets the bottom of the micropattern once it makes contact with it. However, in the case of two level topography (micro-Cassie/nano-Cassie transition) the bottom and the sidewalls are coated with superhydrophobic nanofilaments which have a very high advancing contact angle. In this case, there remain ring-shaped air pockets around the bases of the posts (a micrograph is shown in Fig. S2).

Fig. S1*C* depicts the situation. After the transition to nano-Cassie state, while the pressure is still on, the contact angle at the post sidewall and at the bottom equals $\theta_A$. Applying Eq. **S7** with $\alpha = \theta_A$ and $\theta = \theta_A$ we get

$$r = \frac{\gamma}{\Delta p}\left[-\sin\theta_A + \sqrt{\sin^2\theta_A - \frac{r_p\Delta p}{\gamma}\left(2\cos\theta_A - \frac{r_p\Delta p}{\gamma}\right)}\right], \qquad [S10]$$

which gives the width of the air pocket as $r - r_p$. For $\Delta p = 7$ kPa, i.e., just enough to cause a transition to nano-Cassie state, the width of the air pockets would be 4.6 μm (with $r_p = 5$ μm and $\theta_A = 170°$). We can thus see that a larger pressure is needed to wet most of the bottom (Fig. S1*D* shows the shape of the air pocket with $\Delta p = 10$ kPa). The pocket width always has a finite value with any $\Delta p$, so at least in theory there always remains an air pocket. On the other hand, we can see from Eq. **S7** that with $\Delta p \geq 0$ one must have $\cos\theta < -\sin\theta$ (i.e., $\theta_A < 135°$) for an air pocket to exist. Therefore air pockets will not be found on single level topographies.

When Laplace pressure is removed, the air pocket assumes a zero curvature shape (see Fig. S1*D* for an example). The receding contact angle $\theta_R$ of the nanocoating dictates the minimum width

the pocket must have in the final state. Using [S7] with $\Delta p = 0$, we find

$$r_{\min} = -\frac{\cos\theta_R}{\sin\theta_R} r_p. \qquad \text{[S11]}$$

If $r_{\min}$ is large enough, the air pockets of adjacent posts coalesce and the nano-Cassie state becomes unstable. This will happen if

$$\cos\theta_R \le -\left(\frac{r_p^2}{(L/2)^2} + 1\right)^{-\frac{1}{2}}, \qquad \text{[S12]}$$

where $L$ is the pitch of the micropattern. For the geometry used in this study we find that the air pockets coalesce for receding angles more than 153.4°. In other words, too hydrophobic a nanopattern leads to an unstable nano-Cassie state.

**Negative Laplace Pressure and Reverse Transition.** When a negative Laplace pressure is produced by suction, the air pockets at the bases of the posts begin to expand, governed by the magnitude of $\Delta p$ and $\theta_R$. An example shape is shown in Fig. S1*D*. The width of the air pocket is determined by equation similar to [**S10**]:

$$r = \frac{\gamma}{\Delta p}\left[-\sin\theta_R \pm \sqrt{\sin^2\theta_R - \frac{r_p\Delta p}{\gamma}\left(2\cos\theta_R - \frac{r_p\Delta p}{\gamma}\right)}\right]. \qquad \text{[S13]}$$

Of the two solutions the one corresponding to a minus sign can be deemed unphysical because with $\Delta p \to 0^-$ we would have $r \to \infty$. The physical solution (corresponding to plus sign) is consistent with [**S11**] with $\Delta p = 0$ and increases with decreasing pressure. However, a negative enough pressure renders the determinant (expression under square root) negative, restricting the maximum size of the air pocket.

With a negative $\Delta p$, the air pocket can be destabilized by two ways. First, the determinant in Eq. **S13** may become negative implying that no stable solution exist. This occurs with pressures lower than

$$\Delta p_{c,1} = \frac{\gamma}{r_p}\left(\cos\theta_R - \sqrt{2\cos^2\theta_R - 1}\right). \qquad \text{[S14]}$$

However, if the air pockets grow large enough to coalesce before $\Delta p_{c,1}$ is reached, they become unstable at a pressure less negative than $\Delta p_{c,1}$. Depending on $\theta_R$, this will happen if the radius corresponding to $\Delta p_{c,1}$ is larger than $L/2$. The receding angle value $\theta_R^*$ for which $r = L/2$ at $\Delta p_{c,1}$ is given by the equation

$$\sin\theta_R^* = \frac{L/2}{r_p}\left(\cos\theta_R^* - \sqrt{2\cos\theta_R^* - 1}\right). \qquad \text{[S15]}$$

With $\theta_R > \theta_R^*$, the air pockets will coalesce at the Laplace pressure

$$\Delta p_{c,2} = -\frac{2\gamma}{r_p}\frac{\frac{L/2}{r_p}\sin\theta_R + \cos\theta_R}{\left(\frac{L/2}{r_p}\right)^2 - 1}. \qquad \text{[S16]}$$

The actual critical pressure for the nano-Cassie to micro-Cassie transition can thus be written as

$$\Delta p_c = \begin{cases} \Delta p_{c,1} & \text{if } \theta_R < \theta_R^* \\ \Delta p_{c,2} & \text{if } \theta_R > \theta_R^* \end{cases} \qquad \text{[S17]}$$

$\Delta p_c$ depends strongly on $\theta_R$ and obviously goes to zero when equality in [**S12**] applies. In this study, $\Delta p_c$ ranges between −5.0 kPa and −1.3 kPa (corresponding to $\theta_R = 145 \pm 5°$).

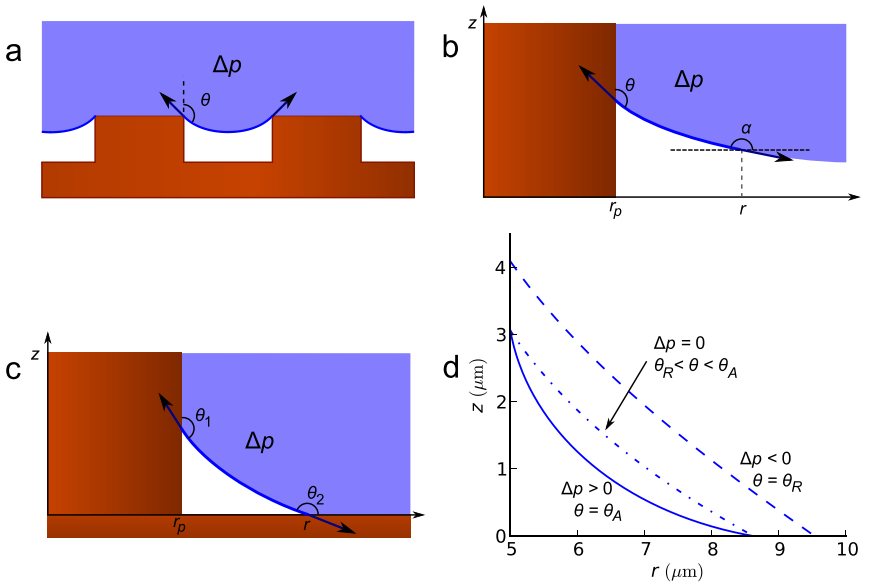


**Fig. S1.** Microscopic meniscus shape. (*A*) Deformation of the meniscus under Laplace pressure. The surface tension counters the force caused by pressure. (*B*) Schematic representation of Eq. **S7** in *SI Text*. (*C*) An air pocket at the base of a post. (*D*) Air pocket shapes calculated by integrating Eq. **S9**. From *Left* to *Right*: Δp = 10 kPa, the state after the water has been pushed between the posts by pressure ($\theta_A = 170°$); Δp = 0, the pressure has been released; Δp = −3 kPa, negative pressure is generated by suction ($\theta_R = 145°$).

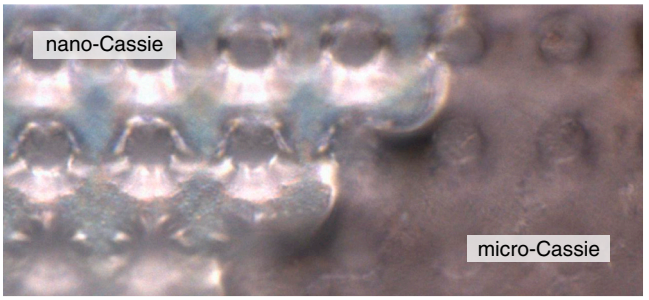


**Fig. S2.** An optical micrograph of a micro-Cassie/nano-Cassie boundary. The sample is tilted by 22° so that horizontal water-air interfaces do not reflect incident light to the objective. Consequently interfaces with a nonhorizontal slope appear brightest. Due to this, the air pockets at the bases of the posts are shown clearly. It is also obvious that the nano-Cassie region is much brighter overall due reflections from the interfaces between the air pockets and water. Because of the tilt and the shallow depth of field of the objective, only one row of posts is in focus in the image.

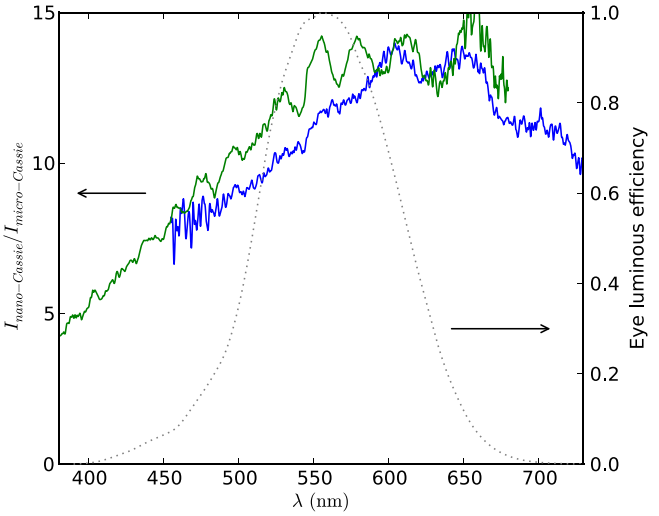


**Fig. S3.** Light scattering contrast. Solid lines: the light scattering intensity ratio $I_{nano\text{-}Cassie}/I_{micro\text{-}Cassie}$ as a function of wavelength (blue curve measured with a tungsten light source, green curve measured with a mercury-vapor light source). Dotted line: eye sensitivity (photopic function, source: http://www.cvrl.org/lumindex.htm). In the range where eye is sensitive the nano-Cassie state scatters 8–14 times more than the micro-Cassie state.

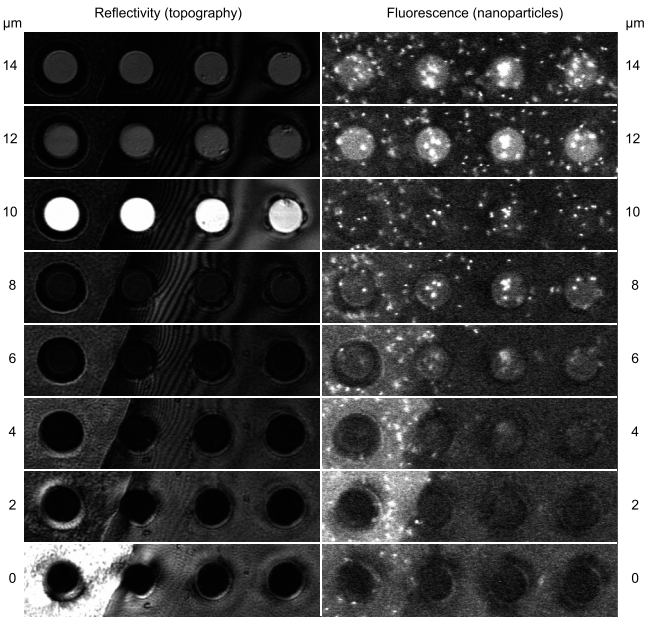


**Fig. S4.** Original confocal microscopy data without noise removal or contrast adjustment. Images were taken every 1 μm, but only every other image is shown here to conserve space. Conventional reflectivity scan is shown on the *Left*, while fluorescence signal from nanoparticles is shown in the *Right*.